Article

Targeting Exposed Phosphatidylserine Enables the Clear Demarcation of Brain Metastases in Mouse Models

Lulu Wang , Alan H. Zhao , Chad A. Arledge , Fei Xing , Michael D. Chan , Rolf A. Brekken , Amyn A. Habib , Dawen Zhao *

Posted Date: 15 August 2024

doi: 10.20944/preprints202408.1163.v1

Keywords: phosphatidylserine (PS); brain micrometastases; vascular endothelial cells; bloodtumor-barrier (BTB); imaging

 doi:10.20944/preprints202408.1163.v1

Article

Targeting Exposed Phosphatidylserine Enables the Clear Demarcation of Brain Metastases in Mouse Models

Lulu Wang [1], Alan H. Zhao [2], Chad A. Arledge [1], Fei Xing [3], Michael D. Chan [4], Rolf A. Brekken [5], Amyn A. Habib [6] and Dawen Zhao [1,3,7,*]

1 Department of Biomedical Engineering, Wake Forest University School of Medicine, Winston-Salem, NC.
2 University of North Carolina School of Medicine, Chapel Hill, NC.
3 Department of Cancer Biology, Wake Forest University School of Medicine, Winston-Salem, NC.
4 Department of Radiation Oncology, Wake Forest University School of Medicine, Winston-Salem, NC.
5 Department of Surgery, Hamon Center for Therapeutic Oncology Research, UT Southwestern Medical Center, Dallas, TX.
6 Department of Neurology, UT Southwestern Medical Center and the North Texas VA Medical Center, Dallas, TX.
7 Department of Translational Neuroscience, Wake Forest University School of Medicine, Winston-Salem, NC.
* Correspondence: dawzhao@wakehealth.edu; Tel.: +13367135783.

Simple Summary: Prognosis of brain metastasis is extremely poor, partly because of concurrence of multiple brain lesions and their limited access to current systemic therapies. Applying a phosphatidylserine (PS)-targeting antibody, we identified abundant PS on the vasculature of brain metastases in mouse models. Given its location on the luminal surface of tumor blood vessels, exposed PS appears to be an ideal target for both diagnostic and therapeutic agents, which otherwise have difficulty penetrating the blood-tumor-barrier (BTB) of brain metastases.

Abstract: Brain metastasis is the most common intracranial malignancy in adults. The prognosis is extremely poor, partly because most patients have more than one brain lesion, and the currently available therapies are nonspecific or inaccessible to those occult metastases due to an impermeable brain-tumor-barrier (BTB). Phosphatidylserine (PS) is externalized on the surface of viable endothelial cells (ECs) in tumor blood vessels. In this study, we have applied a PS-targeting antibody to assess brain metastases in mouse models. Fluorescence microscopic imaging revealed that extensive PS exposure was found exclusively on vascular ECs of brain metastases. The highly sensitive and specific binding of the PS antibody enables individual metastases, even micrometastases containing an intact BTB, to be clearly delineated. Furthermore, conjugation of the PS antibody with a fluorescence dye, IRDye 800CW, or a radioisotope, ^{125}I, allowed clear visualization of individual brain metastases by optical imaging and autoradiography, respectively. In conclusion, we demonstrated a novel strategy of targeting brain metastases based on our finding that abundant PS exposure occurs on blood vessels of brain metastases but not normal brain, which may be useful for the development of imaging and targeted therapeutics for brain metastases.

Keywords: phosphatidylserine (PS); brain micrometastases; vascular endothelial cells; blood-tumor-barrier (BTB); imaging

1. Introduction

Brain metastasis is the most frequently occurring intracranial malignancy in adults [1,2]. The incidence of brain metastasis seems to have increased over the past decade and may be the paradoxical result of the effectiveness of drugs on primary cancer. In part, this is due to the fact that

 doi:10.20944/preprints202408.1163.v1

chemotherapeutic agents that show efficacy against systemic disease have poor penetration of the blood-tumor-barrier (BTB), which means that brain metastases are significantly undertreated [3–6]. Many brain metastasis patients exhibit multiple tumors at the time of diagnosis. Even in the event of a solitary metastasis, it is believed that the brain may be seeded with many radiographically invisible metastases [7,8]. Whole brain radiation therapy (WBRT) alone or in combination with surgical resection or stereotactic radiosurgery is thus the standard of care for brain metastasis patients. However, WBRT is often associated with neurological complications that preclude sufficient radiation doses to effectively treat the lesions. The prognosis for brain metastasis is extremely poor, with a median survival of 8-16 months even with combination treatment [9,10]. Thus, there is an urgent need to develop new diagnostic and therapeutic agents that are specific and effective for brain metastases.

Multiple strategies have been exploited to improve brain metastases access to systemic diagnostic and therapeutic agents [11,12]. However, limited success has been reported with the physical or chemical approaches to open BTB, primarily owing to inhomogeneous disruption of BTB and more importantly, unwanted damage of blood-brain-barrier (BBB) in normal brain, resulting in neurological toxicity from drugs or blood components entering the normal brain [6]. Taking advantage of intravascular receptors that mediate transcytosis across the BBB, several ligands or antibodies that specifically bind to such receptors have been conjugated directly or indirectly with therapeutic compounds [13]. Despite leading to increased drug concentrations to brain tumors, this strategy also causes toxicity to normal brain because the receptors such as transferrin, insulin and low-density lipoprotein receptor are widespread in normal brain [14]. Clearly, discovery of a biomarker that is specific to brain metastasis will be critical for the development of brain metastasis-targeted diagnosis and therapy. Ideally, this biomarker needs to be accessible to systemically administered diagnostic and therapeutic agents. Thus, a vascular luminal surface-exposed biomarker might be particularly useful for developing brain metastasis-targeting agents, which otherwise have difficulty passing through the BTB to brain metastases.

Phosphatidylserine (PS), the most abundant anionic phospholipid of the cell membrane, is normally constrained to the inner leaflet of the plasma membrane of healthy cells. PS becomes externalized on the outer leaflet of the plasma membrane of cells during programmed cell death, apoptosis. However, PS exposure can occur in endothelial cells of tumor blood vessels and cancer cells [15,16]. These cells are viable and PS exposure is inducible and reversible, which is distinct from the irreversible process of PS externalization during apoptosis [17–19]. We and others have previously reported various levels of PS-positive tumor blood vessels, ranging from 5% to 40% among multiple tumor models [20,21].

In the present study, we applied a monoclonal PS-targeting antibody, 1N11 to assess PS exposure on vasculature of brain metastases in mouse models. After systemic administration of 1N11, PS exposure on tumor vascular ECs was quantified by detecting 1N11+ CD31+ ECs with fluorescence microscopy imaging. Notably, 1N11+ fluorescence signal was only seen in brain metastases, coinciding well with CD31+ tumor vascular ECs. Examination of series of whole mount brain sections revealed that 1N11+ fluorescence signals clearly demarcated individual brain metastases. Since previous works suggest that PS exposure in non-apoptotic cells is possibly caused by oxidative stresses in the tumor microenvironment (TME), we investigated plausible contribution of oxidative stress-related factors including tumor hypoxia and inflammatory cytokines, tumor necrotic factor (TNF-α) and interleukin (IL)-1. To investigate the potential of targeting exposed PS for sensitive and specific imaging of brain metastases, we labeled 1N11 with a fluorescence dye, IRDye 800CW, or a radiotracer, I-125, to perform optical imaging and autoradiographic imaging of brain metastases in mice.

 doi:10.20944/preprints202408.1163.v1

2. Materials and Methods

2.1. Reagents and Cell Lines

The human monoclonal antibody, 1N11, binds to PS, while Aurexis, a human monoclonal antibody, binds to an irrelevant antigen (*S. aureus* clumping factor A), serving as a negative control antibody. Both antibodies were generously provided by Drs. Philip Thorpe and Rolf Brekken (UT Southwestern Medical Center at Dallas). Murine breast cancer 4T1 cells and human umbilical vein endothelial cells (HUVEC) were purchased from American Type Culture Collection (ATCC, Manassas, VA). The brain-tropic human breast cancer MDA-MB-231/BR-GFP (231-Br) cell line was a kind gift from Dr. Patricia Steeg (NIH/NCI).

2.2. Breast Cancer Brain Metastasis Models

All animal procedures were approved by the Institutional Animal Care and Use Committee of Wake Forest University School of Medicine and University of Texas Southwestern Medical Center. Murine breast cancer 4T1 cells and brain-tropic human breast cancer 231-Br cells were incubated in Dulbecco's modified Eagle's medium (DMEM) with 10% FBS, 1% L-Glutamine and 1% penicillin-streptomycin at 37°C with 5% CO_2. Once 80% confluence was reached, the cells were harvested, and suspended in serum-free medium. Immunocompetent female BALB/c mice (n = 6; 6-8 weeks old; NCI, Frederick, MD) were used for the 4T1 model, while female nude mice (n = 16; BALB/c nu/nu, 6-8 weeks old; NCI or The Jackson Laboratory) were used for the human breast cancer 231-Br model. The mice were anesthetized with inhalation of 2% isoflurane. 2×10^5 4T1 cells or 231-BR cells (in 100 μl of serum free medium) were injected directly into the left ventricle of a mouse heart under the imaging guidance of a small animal ultrasound (Vevo 770, VisualSonics; Toronto, Canada).

2.3. Longitudinal MRI Monitoring of Development of Brain Metastases

MRI was initiated two weeks after tumor implantation and repeated once a week for up to three weeks. Animals were sedated with 3% isoflurane and maintained under general anesthesia (1.5% isoflurane). Animal body temperature and respiration were monitored and maintained constant throughout the experiment. MR measurements were performed using a 9.4T horizontal bore magnet with a Varian INOVA Unity system (Palo Alto, CA) or a 7T Bruker BioSpec 70/30 USR scanner (Bruker Biospin, Rheinstetten, Germany). A tail vein of mouse was catheterized using a 27G butterfly for Gd-DTPA (Magnevist®; Bayer HealthCare, Wayne, NJ) contrast agent administration. High resolution multi-slice (14 slices with 1mm-thick) T_2-weighted coronal images, covering from the frontal lobe to the posterior fossa, were acquired with fast spin echo multiple slice sequence (TR/TE = 2500 ms/48 ms, 8 echo trains, matrix: 256 x 256, FOV 20 x 20 mm, resolution: 78 x 78 μm^2 in plane). T_1-weighted contrast enhanced images were acquired with spin echo multi-slice sequence (TR/TE = 400 ms/20 ms, matrix: 256 x 256, FOV 20 x 20 mm). We determined tumor volume on T_2-weighted images by manually outlining the enhancing portion of the mass on each image by using standard ''browser'' software provided with the Varian Inova imaging system or the Bruker system.

2.4. Detection and Quantification of Exposed PS In Vivo

Immediately after the last MRI follow-up of the 231-Br mice (n=6), 150 μg of 1N11 or the control body Aurexis were injected *i.v.* and allowed to circulate for 4 h. The mice were anesthetized, exsanguinated, and perfused with heparinized saline. The mouse brains were dissected and frozen for preparation of cryosections. We analyzed the entire brain of each animal by immunohistochemistry. Vascular endothelium was stained using a rat anti-mouse CD31 antibody (1:20; Serotec Inc., Raleigh, NC, USA) followed by Alexa Fluor 350-labeled goat anti-rat IgG (1: 200; BD Biosciences, San Jose, CA). 1N11 or Aurexis was detected using goat anti-human IgG conjugated to Cy3 (1:500; Jackson Immunoresearch Laboratory, West Grove, PA). The immunostained sections of the entire brain were evaluated under Zeiss LSM510 (Carl Zeiss MicroImaging, Inc., Thornwood, NY), and the individual 10× fluorescence images were automatically stitched by using SoftWoRx

 doi:10.20944/preprints202408.1163.v1

(Applied Precision, Issaquah, WA). Doubly labeled endothelial cells (i.e. CD31 positive/1N11 positive) were identified on merged images. The percentage of doubly positive vessels was calculated as follows: (mean number of yellow vessels per field/mean number of total vessels) × 100. Ten random fields containing metastases were evaluated for each section.

2.5. Immunohistochemical Detection of Hypoxia and TNF-α in Brain Metastasis

To detect hypoxia, pimonidazole (60 mg/kg, Hypoxyprobe, Burlington, MA) was injected intravenously 60 mins before sacrifice. Pimonidazole was recognized by primary Mab1 (1:100; Hypoxyprobe) and followed by rabbit anti-mouse secondary conjugated to AMCA (1:300; Jackson Immunoresearch Laboratory). For TNF-α staining, anti-TNF-α (1:200; R&D Systems) was followed by horseradish peroxidase (HRP)-conjugated goat anti-rat secondary antibody (1:1000; Santa Cruz Biotechnology). After a PBST wash, sections were immersed in DAB (3,3′-diaminodbenzidine; Thermo Fisher Scientific) and then observed under microscope.

2.6. Near Infrared Fluorescence Imaging

1N11 and Aurexis F(ab')$_2$ fragments were generated by reacting antibodies with pepsin at a molar ratio of 1:130 (antibody:pepsin) for 1 h at 37^{o}C. F(ab')$_2$ fragments (MW = 110 kDa) were purified by FPLC using an S-200 column (Pharmacia, Piscataway, NJ) and PBS running buffer. F(ab')$_2$ was then reacted with an N-hydroxysuccinimide ester derivative of IRDye 800CW (Li-COR, Lincoln, NE) at molar ratio of 1:10 (F(ab')$_2$:dye) for 2 h at room temperature. Unreacted dye was separated from the conjugate using a PD-10 desalting column (GE Healthcare, Uppsala, Sweden). Analyses of the final product, based on the absorbance of the dye at 778 nm and the absorbance of the F(ab')$_2$ at 280 nm, showed that it consisted of approximately 2 molecules of dye bound to each F(ab')$_2$ fragment. The products are referred to as 800CW-1N11 or 800CW-Aurexis throughout this manuscript. Immediately after the last MRI follow-up at 5 weeks post intracardiac injection, 800CW-1N11 or 800CW-Aurexis (2 nmol/mouse) was injected into a tail vein of the brain metastasis mice. Twenty-four hours later, the mice were sacrificed and perfused, and brains were dissected. *Ex vivo* fluorescence imaging (excitation, 671-705 nm; emission, 730-950 nm) was performed using a Maestro imaging system (CRI Inc. Woburn, MA). Brain tissues were then embedded in optimal cutting temperature compound (O.C.T.) and then transferred to –80^{o}C freezer. On the second day, a series of coronal sections (10 μm) of the entire brain was cut with a cryostat. The sections containing tumor tissues were identified by H&E staining. The adjacent frozen sections were then used for *ex vivo* fluorescence imaging. The *ex vivo* images of the thin frozen sections were acquired by the same Maestro system. Typically, an exposure time of 2.0 s was applied for image acquisition. Fluorescence images were processed with the Maestro software 2.8. Lastly, the frozen sections were then stained with anti-CD31 and correlated with the 800CW-1N11 signals using an Envos microscope (AMG, Bothell, WA) equipped with near-infrared (NIR) filters.

2.7. Autoradiographic Imaging of I-125 Labeled 1N11

Iodine-125 (^{125}I) was purchased from Perkin Elmer (Waltham, MA). Pre-coated iodination tubes and Protein A agarose were from Pierce Biotechnology (Rockford, IL). Instant thin-layer chromatography plates (ITLC-SG) were from Pall Life Sciences (East Hills, NY). F(ab')$_2$ fragments were generated by reacting antibodies with pepsin at a molar ratio of 1:130 (antibody:pepsin) for 1 h at 37^{o}C. F(ab')$_2$ fragments were purified on a FPLC S-200 column (Pharmacia, Piscataway, NJ). The F(ab')$_2$ fragments were then radioiodinated using the indirect IODO-GEN method (Pierce Biotechnology). Briefly, 1-3 mCi of iodine were activated in 100 μl iodination buffer (125 mM Tris-HCL, pH 6.8, 150 mM NaCl) in a pre-coated iodination tube and then reacted with 0.2-0.6 mg F(ab')$_2$ in 100 μl iodination buffer in a separate uncoated tube. Free iodine was removed with Bio-Spin 6 gel filtration columns (Bio-Rad Laboratories, Hercules, CA) that were pre-blocked with iodination buffer containing 10% FBS. Radio-TLC analysis was used to determine iodination efficiency on a Rita Star Radioisotope TLC Analyzer (Straubenhardt, Germany) using ITLC-SG plates. Immediately after

 doi:10.20944/preprints202408.1163.v1

anatomic MRI, each mouse was given i.v. 60 μCi ^{125}I-1N11 F(ab')$_2$. Forty-eight hours later, the mice were perfused, and mouse brains were dissected. Using a mouse brain matrix, 4 mm-thick brain bearing brain metastases, correlating with the MRI, were cut from each mouse brain and laid on an autoradiographic film. After 12 h incubation, the film was read using Cyclone Plus Storage Phosphor (PerkinElmer, Waltham, MA). Spatial localizations of 'hot spots' on radiographic images were correlated with MRI stacked images. Signal intensity of the tumor versus normal brain was also calculated.

2.8. Statistical Analysis

Statistical analysis was performed using Microsoft Excel. Data were presented as mean ± SD. Statistical significance was determined by Student's t test. All t tests were one-tailed, unpaired and considered statistically significant if $p < 0.05$.

3. Results

3.1. MRI Detects Brain Metastases and Evaluates the BTB Permeability

Longitudinal MRI was performed to detect and follow up the intracranial development of brain metastases in mice. As shown in **Figure 1**, multi-focal brain metastases started to appear on T_2-weighted images 3 weeks after intracardiac injection of 231-Br cells, many of which became apparently larger on the follow-up MRI at week 4. T_1-w contrast enhanced images at the initial scan revealed a small fraction of the lesions with high signal intensity, although the number of the enhanced lesions increased at the follow-up scan, which indicated that the BTB in many brain metastases was intact (**Figure 1a**). For a total of 464 brain metastases that were identified on T_2-w images, only 160 of them were found to be permeable to MRI contrast agent, Gd-DTPA (**Figure 1b**). Interestingly, our data showed that there was no significant correlation between tumor volume and the BTB permeability (**Figure 1b**). In a good agreement with previous studies by others and us [6,22–25], these data clearly showed the heterogeneous BTB permeability among individual brain metastases and the evolution of the BTB disruption with intracranial growth of the metastases.

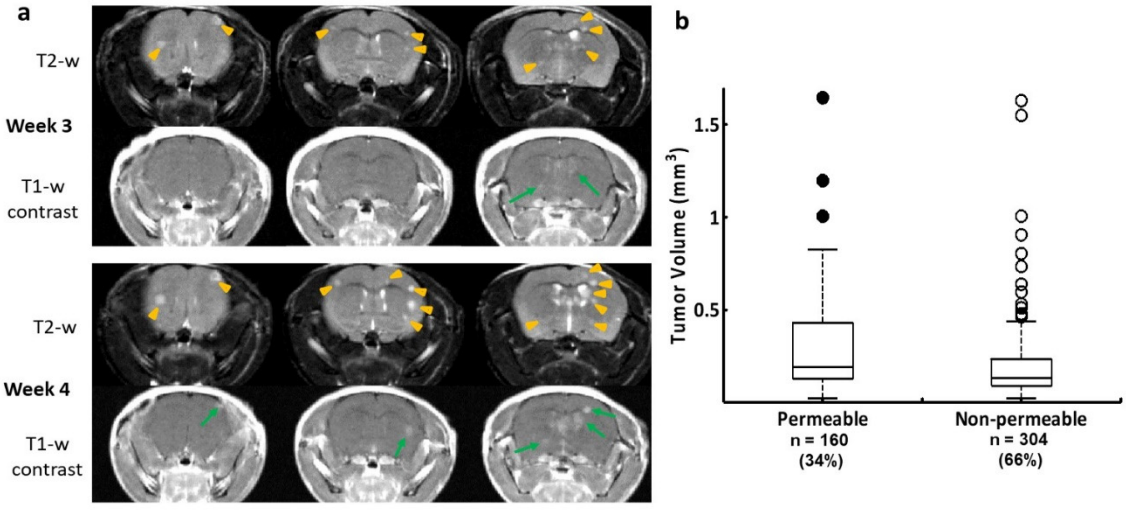

Figure 1. Longitudinal MRI monitoring of intracranial distribution of brain metastases and permeability of the BTB in the 231-Br model. **a.** Three consecutive coronal sections of high-resolution MRI were obtained from a representative mouse brain bearing 231-Br metastases. At week 3, T_2-w images revealed multiple hyperintense metastases across the brain (yellow arrowheads), only two of which were enhanced on T_1-w post contrast images (green arrows), indicating a leaky BTB. At week 4, several new lesions appeared on T_2-w images (yellow arrowheads), while those lesions seen on the prior scan became larger. An increased number of the contrast enhanced lesions were seen at this time (green arrows). **b.** A total of 464 231-Br brain metastases were identified by MRI including non-

 doi:10.20944/preprints202408.1163.v1

permeable (n = 304) and permeable (n = 160) metastases based on T_1-w post contrast images. A plot of permeability versus size indicated that larger metastases tend to be leaky. However, there was no significant difference in tumor size between the permeable and non-permeable metastases (p = 0.1).

3.2. PS Externalization in Vascualr ECs of Brain Metastases But Not Normal Brain

The 231-Br model was used in this study, and MRI scans were performed to confirm the intracranial development of multiple brain metastases and heterogeneous permeability in the BTB of individual brain metastases (**Figure 2a**). Immediately after MRI, 1N11 or Aurexis (150 μg) were injected intravenously into 231-Br mice. Four hours later, the mice were exsanguinated and perfused to wash out unbound antibodies in the circulation. H&E-stained brain sections correlated well with MRI, but apparently depicted additional micrometastases that were undetectable by MRI (**Figure 2b, 2c**). Immunohistochemical staining of 1N11 was then performed on frozen sections of the entire mouse brain, which were also co-stained with anti-CD31 antibody for vascular endothelial cells (**Figure 2d-j**). As shown in **Figure 2d**, fluorescence microscopic imaging revealed extensive 1N11 positive regions on a whole brain section, which coincided with individual metastases identified on the H&E staining (**Figure 2c**), including micrometastases (**Figure 2d**). The superior fluorescence contrast demarcated every tumor lesion from surrounding normal brain (**Figure 2c, 2d**). Higher magnification images further showed that 1N11 co-localized with almost every CD31-positive tumor vessel (**Figure 2g-j**; **Figure 3a-c**). Blood vessels in nearby normal brain were not stained by 1N11 (**Figure 2i, 2j**; **Figure 3c**). In contrast, there was no positive Aurexis signal in brain metastases (**Figure 3d-f**). Thus, staining with 1N11 was antigen specific. Quantitative analysis determined that 93% of blood vessels of brain metastases were found to be PS-positive (**Figure 3g**). Together, our data demonstrate that extensive PS exposure occurs in vascular endothelial cells of brain metastases but nor normal brain, which may serve as a useful biomarker for brain metastases.

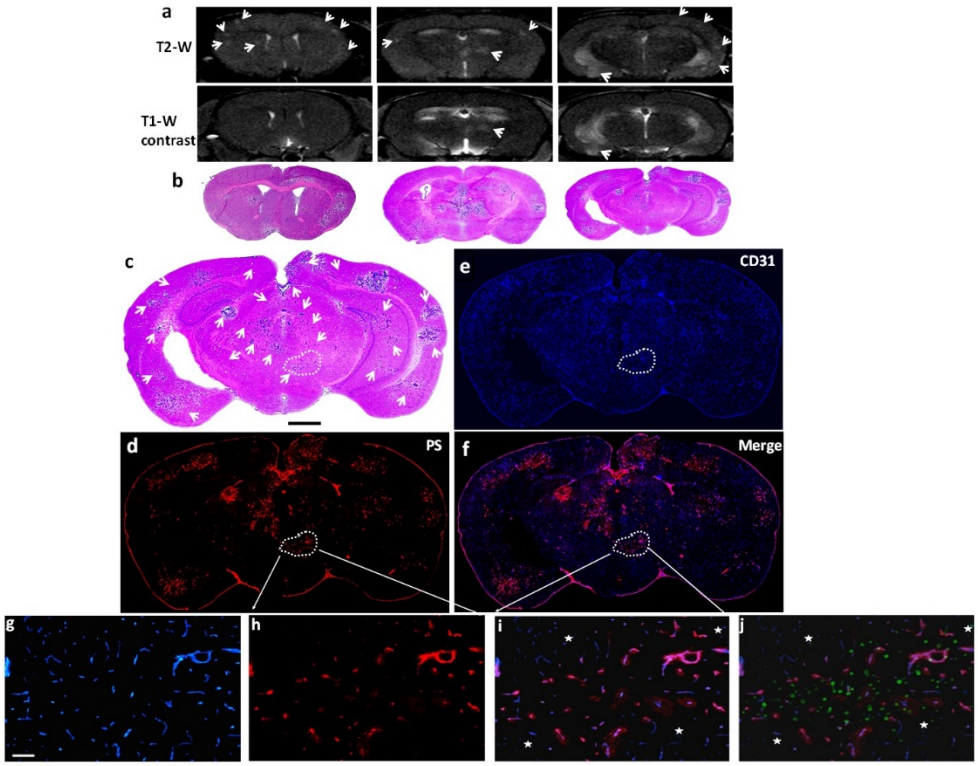

Figure 2. PS exposed exclusively in vascular endothelial cells of brain metastases. **a.** Multiple brain lesions were detected on three consecutive coronal sections of T_2-w images (arrow) in a 231-Br mouse, while a few lesions were enhanced on T_1-w post contrast images (arrow). Immediately after MRI, the mouse was injected i.v. with 1N11 (150 μg). Four hour later, the mouse was perfused and the brain was dissected. **b.** Corresponding H&E sections depicted more microscopic lesions that were invisible

 doi:10.20944/preprints202408.1163.v1

by MRI. **c-f.** Diffuse brain metastases were labeled on one of the H&E sections (arrow; **c**). Immunofluorescence staining on a consecutive section showed that 1N11 (red; **d**) localized to every tumor lesion, even microscopic lesions identified by H&E staining (arrow; bar=1 mm; **c**). Binding of 1N11 to tumor vessels (CD31, blue; **e**) was confirmed by the magenta color in merged images (**f**). **g-j.** A region containing positive 1N11 (outlined in **d**) was selected and magnified (bar = 100 μm). The merged image showed that 1N11 (red, **h**) co-localized with almost every CD31-positive tumor vessel (blue, **g**) to give a magenta color (**i**). Vessels in nearby normal brain (star, **i**) were not stained by 1N11. The tumor regions were distinguished from normal brain by the presence of GFP in the tumor (**j**). .

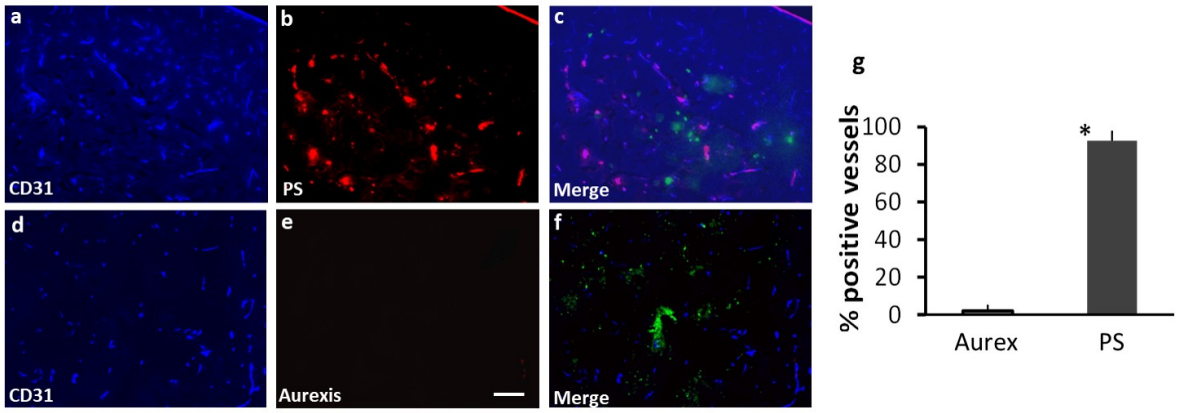

Figure 3. Staining with 1N11 was antigen specific. 213-Br mice were injected i.v. with either 1N11 or the control antibody, Aurexis (150 μg). Four hour later, the mice were perfused and the brains were dissected. **a-c.** A brain region containing a tumor lesion was stained with anti-CD31 for blood vessels (**a**), and co-stained for 1N11 (**b**). The merged image showed that 1N11 co-localized with CD31-positive tumor vessels. Vessels in nearby normal brain (containing no GFP) were not stained by 1N11 (**c**). **d-f.** In contrast, the control antibody, Aurexis, showed no staining of blood vessels of brain metastases (bar = 100 μm)**. g.** For the group of 231-Br mice, the percentage of PS-positive vessels in brain metastases was 93 ± 5%, while only 2 ± 2% for the control antibody Aurexis. * $p < 0.01$.

3.3. Inflammatory Cytokines Are Likely Responsible for PS Exposure in Brain Metastases

It is believed that oxidative stresses such as tumor hypoxia is important in the induction of PS exposure [15,26]. We applied the hypoxic marker, pimonidazole, to study tumor hypoxia in brain metastases. However, there was no positive pimonidazole staining in any of brain metastases (**Figure 4a**). The lack of tumor hypoxia in brain metastases was also reported by Lorger and Felding-Habermann who studied several breast cancer brain metastasis mouse models including the 231-Br model [27]. These data suggest that brain metastases at early stage of development are supplied with adequate oxygen from blood vessels, thus tumor hypoxia is an unlikely contributor to PS exposure in these small brain metastases. Recent studies have reported that inflammatory cytokines such as TNF-α are upregulated in brain metastasis and highly associated with extravasation of cancer cells from blood vessels and their colonization in brain parenchyma [28]. TNF-α signaling is known to generate reactive oxygen species (ROS) [29], and ROS can induce lipid peroxidation in cell membrane and thus changes of membrane properties [30]. Thus, we investigated if TNF-α may induce PS exposure. We treated HUVEC cells with the recombinant TNF-α and stained PS with 1N11. Indeed, abundant PS was detected on the surface of the cells treated with TNF-α but absent in the non-treated cells (**Figure 4b**). We further studied TNF-α expression in brain metastases. Overexpression of TNF-α was consistently evidenced in brain metastases by immunohistochemistry (**Figure 4c**). While such inflammatory cytokine as TNF-α may be linked to PS exposure, we can not rule out plausible contributions from other stress-relevant factors.

 doi:10.20944/preprints202408.1163.v1

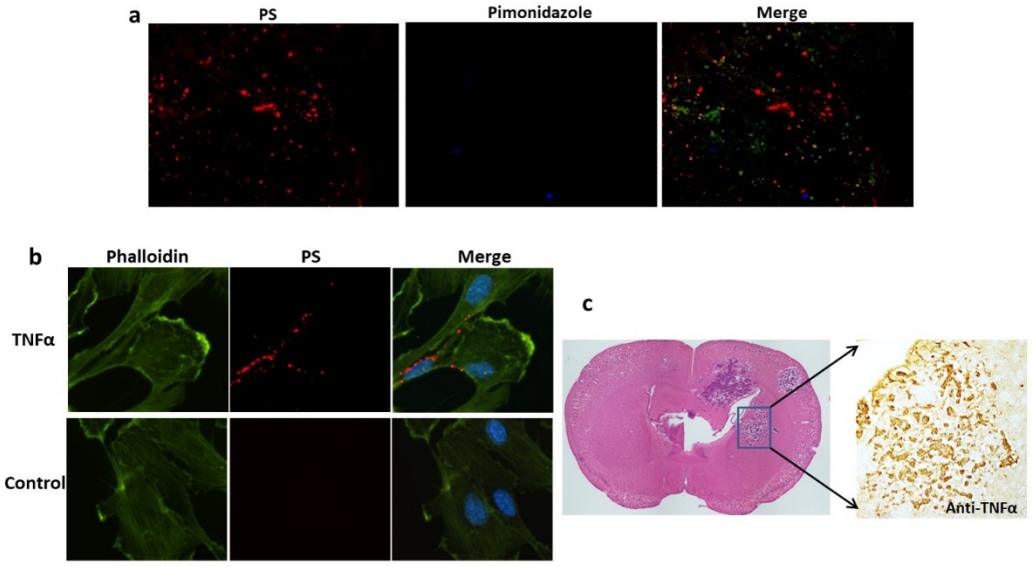

Figure 4. TNF-α induced PS externalization in vascular endothelial cells and overexpression of TNF-α was detected in brain metastases. **a**. A group of 213-Br mice receiving i.v. 1N11 and followed by i.v. pimonidazole were used to study tumor hypoxia. A representative region containing positive 1N11 staining (red) was co-stained for pimonidazole (blue). There was essentially no positive pimonidazole staining in the brain metastasis (GFP). **b.** HUVEC cells were treated with/without TNFα (20 ng/ml) for 24 h before fixation and immunocytostained with 1N11 (red), cytoskeleton (phalloidin, green) and nuclear (DAPI, blue). The merged image showed numerous cell surface-exposed PS in the TNFα-treated cells, while no PS exposure in the control cells. **c.** Anti-TNF-α staining revealed marked expression of TNF-α in the 231-Br brain metastasis but not in normal brains.

3.4. Targeting PS Enables Sensitive and Specific Imaging of Brain Metastases

To explore the possibility of targeting PS for brain metastases imaging, we created the F(ab')$_2$ fragment of 1N11 from the full length 1N11 and then conjugated the 1N11-F(ab')$_2$ with a NIR dye, IRDye800CW to form 800CW-1N11. We applied NIR optical imaging to image the ability of 800CW-1N11 to target exposed PS in brain metastases. In addition to the 231-Br model, we established a brain metastasis model by injecting intracardiacally the murine breast cancer 4T1 cells. Unlike the 231-Br model bearing multifocal brain metastases, the 4T1 model was found to generally form fewer lesions, often a solitary tumor (**Figure 5**). At 24 h after i.v. 800CW-1N11, while NIR imaging of the whole brains revealed multiple regions with high NIR signals in the 231-Br model, a single distinct signal was observed in the 4T1 brain metastasis (**Figure 5a**). To interrogate the brain metastasis-targeting sensitivity and specificity of the 800CW-1N11 imaging, we took a more in-depth look at the signals of 800CW-1N11 throughout the brain sections bearing 4T1 brain metastasis. As shown in **Figure 5b**, a brain lesion appeared on multiple MRI slices, and corresponding H&E sections confirmed the brain metastasis. Ultrathin unstained cryosections (10 μm) adjacent to the H&E sections were then imaged with NIR imaging. Notably, improved contrast of the tumor with distinct tumor margins was detected in each tumor-bearing whole brain section by NIR imaging, which correlated well with histological staining (**Figure 5b**). The ratio of mean signal intensity of tumor to contralateral normal brain, obtained from the ultrathin sections was 5.8, which was significantly higher than that of the control antibody conjugates, 800CW-Aurexis (1.6; $p < 0.05$; **Figure 5c**). Like 1N11 antibody, the majority of 800CW-1N11 was found to bind to tumor vascular endothelial cells, despite some extravascular signals observed under fluorescence microscope (**Figure 5d-f**). The extravascular signals likely resulted from the leakage of 800CW-1N11 via the disrupted BTB, which was evidenced on T_1-w contrast images (**Figure 5b**).

 doi:10.20944/preprints202408.1163.v1

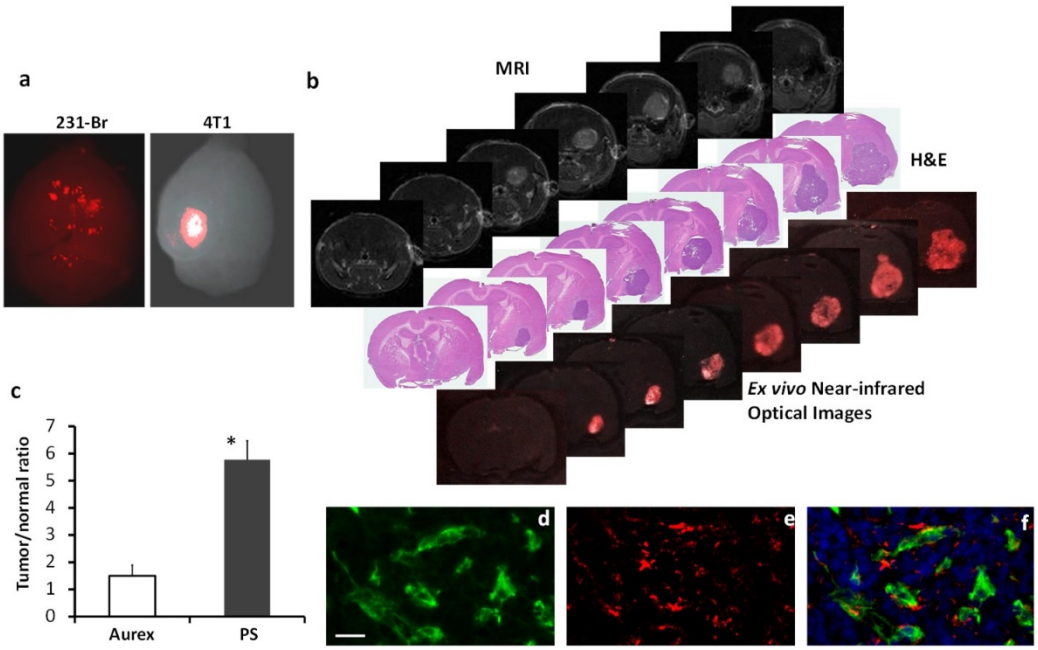

Figure 5. PS-targeted NIR imaging of brain metastases. NIR dye, IRDye-800CW labeled 1N11 F(ab')$_2$, was injected into the mice bearing 231-Br or 4T1 brain metastases. **a.** Twenty-four hours later, *ex vivo* NIR imaging of the whole brain detected distinct 800CW signals from multiple regions of a 231-Br brain, while a clear contrast of a single brain lesion was seen in a 4T1 brain. **b.** A series of unstained coronal brain cryosections (10 μm, bottom row) was obtained after the brain in **a** was imaged. The NIR imaging revealed a clear tumor contrast on the series of brain sections, which correlated well with H&E staining (middle row) of tumors and T1-contrast enhanced MR images (top row). **c.** Quantification of the light intensity in the tumor versus the contralateral normal brain obtained a ratio of 5.7 ± 0.8 with 800CW-1N11, which was significantly higher than that of the control antibody, 800CW- Aurexis (1.5 ± 0.4; * $p < 0.05$). **d.** Tumor vascular endothelial cells were immunostained with anti-CD31 (green) in the cryosections adjacent to those used in **b**. 800CW-1N11 signals (red) from the same field were detected with an NIR filter set (**e**). **f.** The merged image revealed extensive 800CW-1N11 bound to vascular endothelial cells, while some detected in the extravascular space (DAPI, blue).

To further exploit the potential of PS-targeted multimodal imaging, we radiolabeled 1N11 F(ab')$_2$ with iodine-125, ^{125}I-1N11, and injected the conjugates (60 μCi) into a tail vein of the mice bearing 231-Br brain metastases or the healthy mice (**Figure 6a**). Forty-eight hours later, the mice were perfused and mouse brains were dissected. Autoradiography was conducted on 4mm-thick brain sections that aligned with MRI. To enable spatial correlation of the hot spots on autoradiographs (4 mm-thick slice) with tumor lesions on MRI (1 mm-thick slice), 4 consecutive 1 mm MRI images were stacked to generate a synthetic MR image that contained all the tumor lesions from each section **(Figure 6a**). As shown in Figure 6b, the autoradiograph captured multiple hot spots on the tumor-containing brain. Clearly, there was a good spatial correlation between the hot spots on the autoradiograph and tumor lesions on MRI (**Figure 6a, 6b**). In contrast, a clean background devoid of signal was observed on the normal brain **(Figure 6b**). The uptake of ^{125}I-1N11 was significantly higher in the individual lesions than that in normal brain with a ratio of 3.6 ± 0.8 ($p < 0.05$; **Figure 6c**). Taken together, these data demonstrate the high sensitivity and specificity of PS-targeted imaging of brain metastases in the mouse models.

 doi:10.20944/preprints202408.1163.v1

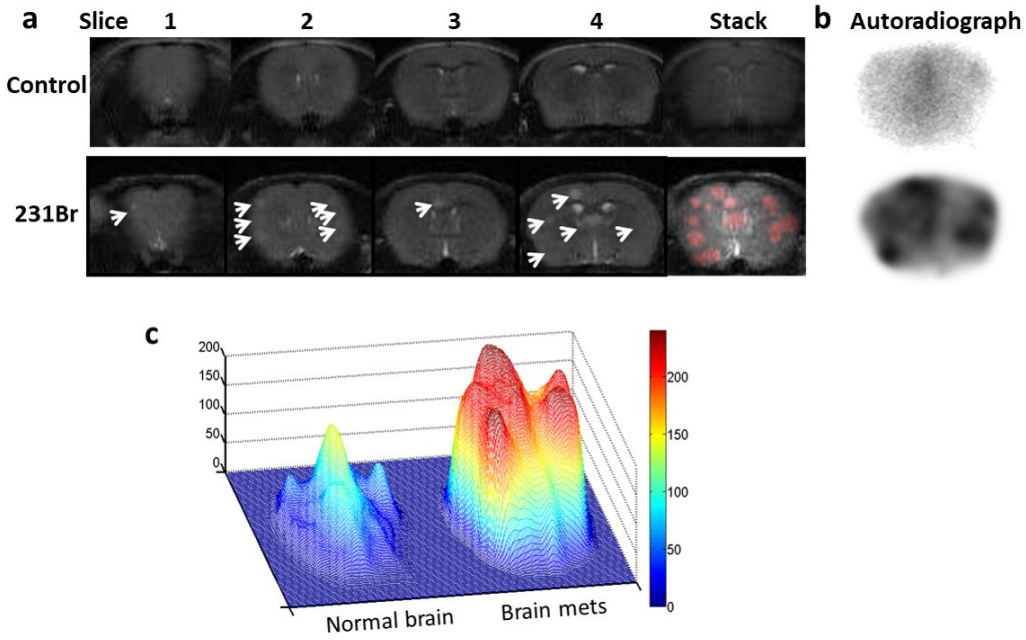

Figure 6. Autoradiography imaging of I-125 labeled 1N11 in targeting brain metastases. **a.** T_2-w MR images of 4 consecutive 1 mm thick coronal slices, covering 4mm brain tissues post bregma, were acquired from a normal control mouse brain (top) and a 231-Br brain (bottom), respectively. Multiple tumors in the 231-Br brain were identified (arrow). An image stack across the 4 slices was created for each animal. For the 231-Br brain, the tumor lesions (red) from each slice were projected on the stacked image to correlate with autoradiography study. **b.** After MRI, each mouse was given i.v. 60 μCi ^{125}I-1N11. Forty-eight hours later, the mice were perfused and mouse brains were dissected. Using a mouse brain matrix, 4mm thick brain tissues post bregma, correlating with the MRI, were cut from each mouse brain and laid the cutting face on the autoradiograph film. After 12 h incubation, autoradiograph images showed multiple hot spots on the tumor brain, while clean background signal was observed on the normal brain. There was a general spatial correlation between tumor lesions on MRI and hot spots on the autoradiograph. **c.** Significantly higher uptake of ^{125}I-1N11 was observed in individual brain metastases, as compared to normal brain tissues (a ratio of 3.6±0.8; $p < 0.05$).

4. Discussion

A significant finding from this study is that abundant PS is externalized on the luminal surface of blood vessels of brain metastases, which can be recognized by the systemically administered PS-targeting antibody. While previous studies reported various levels of PS positive blood vessels among cancer types [20], our data detected PS expression in ~90% of vascular ECs of brain metastases (**Figures 2** and **3**). Importantly, PS exposure was found to be specific to brain metastases since there was no PS detected in normal brain, and the control antibody, Aurexis, showed no positive staining in blood vessels of brain metastases (**Figure 3**). Unlike other tumor models, in which significant angiogenesis commonly leads to enhanced vascular permeability, the intracardiac 231-Br model contains many tumor lesions with an intact BTB, which was found impermeable to the small molecule MRI contrast agent, Gd-DTPA (**Figures 1** and **2**). Along with micrometastases detected by histology, these small lesions may be comparable to those occult brain lesions in human. Notably, positive PS staining co-localized completely with CD31+ tumor vascular ECs. Neither PS antibody nor the control antibody, Aurexis, was seen at extravascular tumor tissues even in those brain metastases that were obviously enhanced by Gd-DTPA (**Figure 2**). These data clearly indicated that biological macromolecules such as proteins were largely inaccessible to tumor parenchyma of the 231-Br brain metastases. These results are in good agreement with previous studies of correlating molecular weight with the BTB permeability in the 231-Br as well as other intracardiac models [6]. Nonetheless, because PS externalization occurred in almost every tumor blood vessel but not normal vessel,

 doi:10.20944/preprints202408.1163.v1

positive immunostaining with the PS-targeting antibody successfully delineated individual brain metastases, even micrometastases, from normal brain tissues (**Figures 2** and **3**).

We further demonstrated the development of PS-targeted imaging probes for sensitive and specific imaging of brain metastases. In addition to the 231-Br model, we also injected murine mammary cancer 4T1 cells intracardiacally into the immunocompetent mice. In contrast to multifocal lesions in the 231-Br mouse brain, fewer lesions, often a solitary lesion, were seen in the 4T1 mouse brain (**Figure 5**). The 4T1 brain metastases were larger and enhanced on T1-w post contrast MRI (**Figure 5b**). Despite most of the 800CW-1N11 probes that were detected on tumor vascular ECs, extravascular signals of 800CW-1N11 were observed (**Figure 5f**), indicating that the BTB disruption is more severe in the 4T1 than the 231-Br brain metastases. Unlike many other cancer biomarkers, which are commonly confirmed with immunohistochemical or biological analyses of tissue specimen from biopsy or resection of a tumor, there is a concern that PS may become externalized during tissue resection and preparation process, and the tissues are no longer suitable for PS detection. Pre-injection of PS antibody to the patient will be necessary for accurate assessment. Alternatively, the development of an optical imaging probe targeting PS, as shown in this study, may be useful for pathological diagnosis of occult metastases. Labeling with a NIR fluorescence dye enables the light to penetrate deeper because it has lower tissue absorption and scattering of light, and is distinct from autofluorescence. Without the use of a secondary antibody for staining, the resected tissue chucks may be screened for the likelihood of brain metastases based on the observation of the optical signals (**Figure 5a**). Subsequent tissue sectioning will likely provide definitive pathological diagnosis in conjunction with routine histology and immunohistochemistry (**Figure 5b**). Moreover, NIR optical imaging has been increasingly applied for intraoperative detection of residual tumors and cancer metastases. The PS-targeting optical probe developed in this study may also be useful for neurosurgeons to identify occult metastases and tumor margins during surgical resection of brain metastasis.

In the present study, we have also labeled 1N11 F(ab')$_2$ with I-125 and successfully applied it for autoradiography imaging of brain metastases, which provided a proof-of-concept for its potential for in vivo nuclear imaging of brain metastases. Indeed, we have previously radiolabeled a PS antibody with ^{74}As, which is a long-lived positron emitter, and used it for PET imaging of prostate tumor in rats [31]. Several other radioisotopes such as ^{64}Cu for PET imaging and ^{111}In for SPECT have also been used to image PS expression in various cancer models [32]. Unlike metabolic radiotracers such as ^{18}FDG for PET imaging, which often gives high signals in normal brain due to a high metabolic rate of neurons, the PS-radioisotope probe is more likely specific to brain metastases because PS exposes only in tumor blood vessels. Other imaging contrast agents may also be considered for attachment to the PS antibody. We have previously attached a MRI contrast agent, iron oxide to the PS antibody and demonstrated its feasibility of imaging tumor vasculature in a breast cancer model [33]. Thus, it will be interesting to explore the utility of the PS-targeted imaging probes for PET/SPECT imaging or MRI of occult brain metastases.

Anti-cancer therapeutic effects of PS-targeting antibody have previously been studied. The antibodies bind to PS-exposed tumor vascular ECs and mediate antibody-dependent cell-mediated cytotoxicity (ADCC) by monocytes and macrophages, resulting in tumor blood vessel collapse and consequently tumor cell starvation and death [34]. The level of PS exposure was found to increase after chemotherapy or radiotherapy, thus a combination with anti-PS antibodies enhanced treatment efficacy [34,35]. Given WBRT being the standard of care treatment for brain metastases in clinic, it will be interesting to investigate the combination of WBRT with anti-PS antibodies in brain metastases. PS is also known for its contribution to anti-inflammatory and immunosuppressed responses through the PS-PS receptor signaling [36,37]. By blocking the interaction, anti-PS antibodies were shown to successfully reprogram the immune cells in the TME and elicit anti-cancer innate and adaptive immunity [36,38,39].

Other strategies may also be considered to exploit PS-targeting antibodies for brain metastases treatment. Alternative to the diagnostic radioisotopes, radiotherapeutic isotopes, such as β⁻emitters, Yttrium-90 (^{90}Y) or Lutetium-177 (^{177}Lu) can be conjugated with PS-targeting antibodies. Advantages

 doi:10.20944/preprints202408.1163.v1

of β^- emitters include their relatively high energy and shorter emission range. After binding to PS on blood vessels of brain metastases, the radiotherapeutics emit high energy to kill tumor vascular ECs and surrounding tumor cells. Importantly, the shorter traveling distance of β^- emitters less likely causes unwanted damage to normal brain. Thus, the development of PS-targeting radiotherapeutics may be particularly useful to target clinically occult brain metastases. Another antibody-based therapeutic strategy is to conjugate the antibody with a chemo-drug. Antibody-drug conjugates (ADCs) have recently shown clinical success in treating several types of cancer. A recent preclinical study reported the efficacy of anti-HER2 antibody-tubulysin ADC on preventing brain metastases of HER2+ breast cancer in mouse models [39]. We consider anti-PS antibody a good candidate for ADC. Moreover, nanoparticle (NPs) delivery systems may have advantages including high drug payload and increased binding affinity due to multiple targeting molecules assembled on the surface of NPs [40–42]. We have recently developed various PS-targeted nano-delivery systems (PS-NPs) by functionalizing the nanoparticles with PS-targeting antibody. While examining different types of PS-NPs, we observed an interesting finding that after binding to the PS exposed cells, the lipid-based nanoparticles (LNPs), but not other types of NP, e.g., iron oxide, became internalized into the targeted cells [33,43–45]. It is believed that binding to the cell surface PS leads to close apposition and subsequent fusion between the lipid layers of LNPs and cell membrane. Thus, we expect that PS-LNP serves as an effective carrier of anti-cancer drugs to brain metastases through the receptor-mediated transcytosis.

Because PS is the same molecule and has the same distribution and regulation in all mammalian species, it is plausible that the mouse data will extrapolate to humans. While exact mechanisms underpinning the high-level expression of PS on blood vessels of brain metastases are unclear, the factors related to oxidative stress and inflammatory cytokines, such as TNF-α overexpression observed in this study (**Figure 4**), are likely playing an important role in flipping PS to the cell surface.

5. Conclusions

In summary, we demonstrate a novel strategy of targeting brain metastases based on our findings that extensive PS exposes on vascular endothelia of brain metastases but not normal brain. The high sensitivity and specificity of PS-targeting antibody enables individual metastases, even micrometastases containing an intact BTB, are clearly delineated. Given its intravascular localization and the lack of a need to cross the BTB, PS appears to be a useful biomarker for the development of imaging and targeted therapeutics for brain metastases.

Author Contributions: Conceptualization, L.W. and D.Z.; methodology, L.W., A.H.Z., C.A.A.; software, L.W., A.H.Z., C.A.A.; formal analysis, L.W., A.H.Z., C.A.A.; investigation, L.W., A.H.Z., C.A.A., D.Z.; resources, R.A.B., D.Z., M.D.C., F.X., A.A.H.; data curation, L.W., A.H.Z., C.A.A.; writing—original draft preparation, L.W., A.H.Z., D.Z.; writing—review and editing, all authors. All authors have read and agreed to the published version of the manuscript. Supervision. F.X., M.D.C., R.A.B., A.A.H.,D.Z.

Funding: This work was supported in part by DOD Breast Cancer IDEA Award W81XWH-08-1-0583 and National Institute of Health/National Cancer Institute 1R01CA264102-01. Imaging was fulfilled by the Southwestern Small Animal Imaging Research Program (U24 CA126608), and the CRi Maestro provided by the Joint Program in BME through a DOE grant #DE-FG02-05CH11280. MRI experiments were performed in the Advanced Imaging Research Center of UTSW, an NIH BTRP # P41-RR02584 facility, and Wake Forest School of Medicine supported by Wake Forest Comprehensive Cancer Center P30 CA01219740. A. A. H. is supported by funding from the National Institutes of Health (No. 1R01CA244212-01A1 and 1 R01 NS119225-01A1).

Institutional Review Board Statement: The animal study protocol was approved by the Institutional Animal Care and Use Committee of Wake Forest University School of Medicine and University of Texas Southwestern Medical Center.

Data Availability Statement: All data are available upon request from the corresponding author.

Acknowledgments: The author would like to pay tribute to the late Dr. Philip Thorpe for his pioneering research on phosphatidylserine and development of a series of PS-targeting antibodies. We thank Drs. Heling Zhou, Srinivas Chiguru, Jason Stafford, Padmakar Kulkarni and Xiankai Sun for technical and collegial support.

 doi:10.20944/preprints202408.1163.v1

Conflicts of Interest: The authors declare no conflicts of interest. UTSW owns multiple patents that cover the use of 1N11 and other PS targeting monoclonal antibodies.

References

1. Wen, P.Y.; Loeffler, J.S. Brain metastases. *Curr Treat Options Oncol* **2000**, *1*, 447-458.
2. Gavrilovic, I.T.; Posner, J.B. Brain metastases: epidemiology and pathophysiology. *J Neurooncol* **2005**, *75*, 5-14.
3. Subramanian, A.; Harris, A.; Piggott, K.; Shieff, C.; Bradford, R. Metastasis to and from the central nervous system--the 'relatively protected site'. *Lancet Oncol* **2002**, *3*, 498-507.
4. Begley, D.J. Delivery of therapeutic agents to the central nervous system: the problems and the possibilities. *Pharmacol Ther* **2004**, *104*, 29-45.
5. Doolittle, N.D.; Abrey, L.E.; Bleyer, W.A.; Brem, S.; Davis, T.P.; Dore-Duffy, P.; Drewes, L.R.; Hall, W.A.; Hoffman, J.M.; Korfel, A.; et al. New frontiers in translational research in neuro-oncology and the blood-brain barrier: report of the tenth annual Blood-Brain Barrier Disruption Consortium Meeting. *Clin Cancer Res* **2005**, *11*, 421-428.
6. Lockman, P.R.; Mittapalli, R.K.; Taskar, K.S.; Rudraraju, V.; Gril, B.; Bohn, K.A.; Adkins, C.E.; Roberts, A.; Thorsheim, H.R.; Gaasch, J.A.; et al. Heterogeneous blood-tumor barrier permeability determines drug efficacy in experimental brain metastases of breast cancer. *Clin Cancer Res* **2010**, *16*, 5664-5678.
7. Steeg, P.S.; Camphausen, K.A.; Smith, Q.R. Brain metastases as preventive and therapeutic targets. *Nat Rev Cancer* **2011**, *11*, 352-363.
8. Eichler, A.F.; Chung, E.; Kodack, D.P.; Loeffler, J.S.; Fukumura, D.; Jain, R.K. The biology of brain metastases-translation to new therapies. *Nat Rev Clin Oncol* **2011**.
9. Gaspar, L.; Scott, C.; Rotman, M.; Asbell, S.; Phillips, T.; Wasserman, T.; McKenna, W.G.; Byhardt, R. Recursive partitioning analysis (RPA) of prognostic factors in three Radiation Therapy Oncology Group (RTOG) brain metastases trials. *Int J Radiat Oncol Biol Phys* **1997**, *37*, 745-751.
10. Lutterbach, J.; Bartelt, S.; Ostertag, C. Long-term survival in patients with brain metastases. *J Cancer Res Clin Oncol* **2002**, *128*, 417-425.
11. Hynynen, K.; McDannold, N.; Vykhodtseva, N.; Jolesz, F.A. Noninvasive MR imaging-guided focal opening of the blood-brain barrier in rabbits. *Radiology* **2001**, *220*, 640-646.
12. Fortin, D.; Gendron, C.; Boudrias, M.; Garant, M.P. Enhanced chemotherapy delivery by intraarterial infusion and blood-brain barrier disruption in the treatment of cerebral metastasis. *Cancer* **2007**, *109*, 751-760.
13. Zhang, Y.; Pardridge, W.M. Blood-brain barrier targeting of BDNF improves motor function in rats with middle cerebral artery occlusion. *Brain Res* **2006**, *1111*, 227-229.
14. Gabathuler, R. Approaches to transport therapeutic drugs across the blood-brain barrier to treat brain diseases. *Neurobiol Dis 37*, 48-57.
15. Ran, S.; Downes, A.; Thorpe, P.E. Increased exposure of anionic phospholipids on the surface of tumor blood vessels. *Cancer Res* **2002**, *62*, 6132-6140.
16. Ran, S.; He, J.; Huang, X.; Soares, M.; Scothorn, D.; Thorpe, P.E. Antitumor effects of a monoclonal antibody that binds anionic phospholipids on the surface of tumor blood vessels in mice. *Clin Cancer Res* **2005**, *11*, 1551-1562.
17. Mirnikjoo, B.; Balasubramanian, K.; Schroit, A.J. Mobilization of lysosomal calcium regulates the externalization of phosphatidylserine during apoptosis. *J Biol Chem* **2009**, *284*, 6918-6923.
18. Balasubramanian, K.; Schroit, A.J. Aminophospholipid asymmetry: A matter of life and death. *Annu Rev Physiol* **2003**, *65*, 701-734.
19. Hammill, A.K.; Uhr, J.W.; Scheuermann, R.H. Annexin V staining due to loss of membrane asymmetry can be reversible and precede commitment to apoptotic death. *Exp Cell Res* **1999**, *251*, 16-21.
20. Ran, S.; Thorpe, P.E. Phosphatidylserine is a marker of tumor vasculature and a potential target for cancer imaging and therapy. *Int J Radiat Oncol Biol Phys* **2002**, *54*, 1479-1484.
21. Zhao, D.; Stafford, J.H.; Zhou, H.; Thorpe, P.E. Near-infrared Optical Imaging of Exposed Phosphatidylserine in a Mouse Glioma Model. *Transl Oncol* **2011**, *4*, 355-364.
22. Zhou, H.; Chen, M.; Zhao, D. Longitudinal MRI evaluation of intracranial development and vascular characteristics of breast cancer brain metastases in a mouse model. *PLoS One* **2013**, *8* e62238.

 doi:10.20944/preprints202408.1163.v1

23. Crowe, W.; Wang, L.; Zhang, Z.; Varagic, J.; Bourland, J.D.; Chan, M.D.; Habib, A.A.; Zhao, D. MRI Evaluation of the effects of Whole Brain Radiotherapy on Breast Cancer Brain Metastasis. *Int J Radiat Biol* **2018**, 1-27.
24. Arledge, C.A.; Sankepalle, D.M.; Crowe, W.N.; Liu, Y.; Wang, L.; Zhao, D. Deep learning quantification of vascular pharmacokinetic parameters in mouse brain tumor models. *FBL* **2022**, *27*.
25. Arledge, C.A.; Crowe, W.N.; Wang, L.; Bourland, J.D.; Topaloglu, U.; Habib, A.A.; Zhao, D. Transfer Learning Approach to Vascular Permeability Changes in Brain Metastasis Post-Whole-Brain Radiotherapy. *Cancers (Basel)* **2023**, *15*.
26. Kirov, A.; Al-Hashimi, H.; Solomon, P.; Mazur, C.; Thorpe, P.E.; Sims, P.J.; Tarantini, F.; Kumar, T.K.; Prudovsky, I. Phosphatidylserine externalization and membrane blebbing are involved in the nonclassical export of FGF1. *J Cell Biochem* **2012**, *113*, 956-966.
27. Lorger, M.; Felding-Habermann, B. Capturing changes in the brain microenvironment during initial steps of breast cancer brain metastasis. *Am J Pathol 176*, 2958-2971.
28. Fares, J.; Cordero, A.; Kanojia, D.; Lesniak, M.S. The Network of Cytokines in Brain Metastases. *Cancers* **2021**, *13*, 142.
29. Kim, J.J.; Lee, S.B.; Park, J.K.; Yoo, Y.D. TNF-α-induced ROS production triggering apoptosis is directly linked to Romo1 and Bcl-XL. *Cell Death & Differentiation* **2010**, *17*, 1420-1434.
30. Cordeiro, R.M. Reactive oxygen species at phospholipid bilayers: Distribution, mobility and permeation. *Biochimica et Biophysica Acta (BBA) - Biomembranes* **2014**, *1838*, 438-444.
31. Jennewein, M.; Lewis, M.A.; Zhao, D.; Tsyganov, E.; Slavine, N.; He, J.; Watkins, L.; Kodibagkar, V.D.; O'Kelly, S.; Kulkarni, P.; et al. Vascular Imaging of Solid Tumors in Rats with a Radioactive Arsenic-Labeled Antibody that Binds Exposed Phosphatidylserine. *Clin Cancer Res* **2008**, *14*, 1377-1385.
32. Gerber, D.E.; Hao, G.; Watkins, L.; Stafford, J.H.; Anderson, J.; Holbein, B.; Oz, O.K.; Mathews, D.; Thorpe, P.E.; Hassan, G.; et al. Tumor-specific targeting by Bavituximab, a phosphatidylserine-targeting monoclonal antibody with vascular targeting and immune modulating properties, in lung cancer xenografts. *Am J Nucl Med Mol Imaging* **2015**, *5*, 493-503.
33. Zhou, H.; Stafford, J.H.; Hallac, R.R.; Zhang, L.; Huang, G.; Mason, R.P.; Gao, J.; Thorpe, P.E.; Zhao, D. Phosphatidylserine-targeted molecular imaging of tumor vasculature by magnetic resonance imaging. *J Biomed Nanotechnol* **2014**, *10*, 846-855.
34. He, J.; Yin, Y.; Luster, T.A.; Watkins, L.; Thorpe, P.E. Antiphosphatidylserine antibody combined with irradiation damages tumor blood vessels and induces tumor immunity in a rat model of glioblastoma. *Clin Cancer Res* **2009**, *15*, 6871-6880.
35. Huang, X.; Bennett, M.; Thorpe, P.E. A monoclonal antibody that binds anionic phospholipids on tumor blood vessels enhances the antitumor effect of docetaxel on human breast tumors in mice. *Cancer Res* **2005**, *65*, 4408-4416.
36. Yin, Y.; Huang, X.; Lynn, K.D.; Thorpe, P.E. Phosphatidylserine-targeting antibody induces M1 macrophage polarization and promotes myeloid-derived suppressor cell differentiation. *Cancer Immunol Res* **2013**, *1*, 256-268.
37. Graham, D.K.; DeRyckere, D.; Davies, K.D.; Earp, H.S. The TAM family: phosphatidylserine sensing receptor tyrosine kinases gone awry in cancer. *Nat Rev Cancer* **2014**, *14*, 769-785.
38. Budhu, S.; Giese, R.; Gupta, A.; Fitzgerald, K.; Zappasodi, R.; Schad, S.; Hirschhorn, D.; Campesato, L.F.; De Henau, O.; Gigoux, M.; et al. Targeting Phosphatidylserine Enhances the Anti-tumor Response to Tumor-Directed Radiation Therapy in a Preclinical Model of Melanoma. *Cell Reports* **2021**, *34*, 108620.
39. Hsiehchen, D.; Beg, M.S.; Kainthla, R.; Lohrey, J.; Kazmi, S.M.; Khosama, L.; Maxwell, M.C.; Kline, H.; Katz, C.; Hassan, A.; et al. The phosphatidylserine targeting antibody bavituximab plus pembrolizumab in unresectable hepatocellular carcinoma: a phase 2 trial. *Nat Commun* **2024**, *15*, 2178.
40. Gril, B.; Wei, D.; Zimmer, A.S.; Robinson, C.; Khan, I.; Difilippantonio, S.; Overstreet, M.G.; Steeg, P.S. HER2 antibody-drug conjugate controls growth of breast cancer brain metastases in hematogenous xenograft models, with heterogeneous blood–tumor barrier penetration unlinked to a passive marker. *Neuro-Oncology* **2020**, *22*, 1625-1636.
41. N'Guessan, K.F.; Davis, H.W.; Chu, Z.; Vallabhapurapu, S.D.; Lewis, C.S.; Franco, R.S.; Olowokure, O.; Ahmad, S.A.; Yeh, J.J.; Bogdanov, V.Y.; et al. Enhanced Efficacy of Combination of Gemcitabine and Phosphatidylserine-Targeted Nanovesicles against Pancreatic Cancer. *Molecular Therapy* **2020**, *28*, 1876-1886.

 doi:10.20944/preprints202408.1163.v1

42. Liu, Y.; Crowe, W.N.; Wang, L.; Petty, W.J.; Habib, A.A.; Zhao, D. Aerosolized immunotherapeutic nanoparticle inhalation potentiates PD-L1 blockade for locally advanced lung cancer. *Nano Res* **2023**, *16*, 5300-5310.
43. Liu, Y.; Wang, L.; Song, Q.; Ali, M.; Crowe, W.N.; Kucera, G.L.; Hawkins, G.A.; Soker, S.; Thomas, K.W.; Miller, L.D.; et al. Intrapleural nano-immunotherapy promotes innate and adaptive immune responses to enhance anti-PD-L1 therapy for malignant pleural effusion. *Nat Nanotechnol* **2022**, *17*, 206-216.
44. Zhang, L.; Zhou, H.; Belzile, O.; Thorpe, P.; Zhao, D. Phosphatidylserine-targeted bimodal liposomal nanoparticles for in vivo imaging of breast cancer in mice. *J Control Release* **2014**, *183C*, 114-123.
45. Wang, L.L.; Habib, A.A.; Mintz, A.; Li, K.C.; Zhao, D. Phosphatidylserine-Targeted Nanotheranostics for Brain Tumor Imaging and Therapeutic Potential. *Molecular Imaging* **2017**, *16*.
46. Zhang, L.; Zhang, Z.; Mason, R.P.; Sarkaria, J.N.; Zhao, D. Convertible MRI contrast: Sensing the delivery and release of anti-glioma nano-drugs. *Sci Rep* **2015**, *5*, 9874.